

## Active shape control of a cantilever by resistively interconnected piezoelectric patches

J. Schoeftner\*<sup>1</sup> and G. Buchberger<sup>2</sup>

<sup>1</sup>*Institute of Technical Mechanics, Johannes Kepler University Linz, A-4040 Linz, Altenberger Str.69, Austria*

<sup>2</sup>*Institute for Microelectronics and Microsensors, Johannes Kepler University Linz, A-4040 Linz, Altenberger Str.69, Austria*

*(Received December 10, 2012, Revised March 25, 2013, Accepted April 5, 2013)*

**Abstract.** This paper is concerned with static and dynamic shape control of a laminated Bernoulli-Euler beam hosting a uniformly distributed array of resistively interconnected piezoelectric patches. We present an analytical one-dimensional model for a laminated piezoelectric beam with material discontinuities within the framework of Bernoulli-Euler and extend the model by a network of resistors which are connected to several piezoelectric patch actuators. The voltage of only one piezoelectric patch is prescribed: we answer the question how to design the interconnected resistive electric network in order to annihilate lateral vibrations of a cantilever. As a practical example, a cantilever with eight patch actuators under the influence of a tip-force is studied. It is found that the deflection at eight arbitrary points along the beam axis may be controlled independently, if the local action of the piezoelectric patches is equal in magnitude, but opposite in sign, to the external load. This is achieved by the proper design of the resistive network and a suitable choice of the input voltage signal. The validity of our method is exact in the static case for a Bernoulli-Euler beam, but it also gives satisfactory results at higher frequencies and for transient excitations. As long as a certain non-dimensional parameter, involving the number of the piezoelectric patches, the sum of the resistances in the electric network and the excitation frequency, is small, the proposed shape control method is approximately fulfilled for dynamic load excitations. We evaluate the feasibility of the proposed shape control method with a more refined model, by comparing the results of our one-dimensional calculations based on the extended Bernoulli-Euler equations to three-dimensional electromechanically coupled finite element results in ANSYS 12.0. The results with the simple Bernoulli-Euler model agree well with the three-dimensional finite element results.

**Keywords:** piezoelastic modeling of a beam; static shape control; dynamic shape control; patch actuators; resistive network; feed-forward control of piezoelastic beam-structures

---

### 1. Introduction

Piezoelectric transducers are extensively used for active and passive vibration control, for structural health monitoring and for energy harvesting. They convert electrical energy into mechanical energy, which allows changing their deformation by applying electrical voltage and vice versa. This effect is exploited when piezoelectric actuators are integrated into an elastic

---

\*Corresponding author, Senior researcher, E-mail: [juergen.schoeftner@jku.at](mailto:juergen.schoeftner@jku.at)

system. These actuators allow for feed-forward vibration control with shape control as a special discipline. The aim of shape control is to achieve a certain displacement field by a proper distribution and actuation of the piezoelectric control agency/-ies if the external loads are known.

The notion shape control has been introduced by Hafka and Adelman (1985). They calculate the temperature field of a supporting structure such that the distortions from the original shape are minimized. Shape control problems belong to the class of so-called inverse mechanical problems where external forces and moment are computed to obtain a desired displacement field, see Irschik (2002). Solutions to this class of problems might not be unique, if they exist: Consider a clamped-clamped slender beam with a constant distribution of the piezoelectric layer. The beam will not vibrate if an electric voltage is applied, see Hubbard and Burke (1992), Irschik, *et al.* (2003) and Irschik, *et al.* (1998). If a shaped layer is added to the constant layer, the response of the beam is solely due to the actuation of the shaped layer. Piezoelectric transducers are often used, especially to control dynamic problems. Nader (2007) verified experimentally the theoretical results for shape control of beam-type structures: if the smart actuation is the negative quasi-static bending moment due to transient imposed forces, the total vertical deflection is zero. In his experimental setup base-excited vibrations of a cantilever are annihilated by actuating a discretized parabolic distribution of piezoelectric patches. Agrawal and Treanor (1999) minimized the integral of the quadratic difference between a desired and an achieved static deflection to obtain the optimized piezoceramics actuator locations and voltages. The concept of shape control is not only restricted to actuated smart structures, it is also possible for passive smart beams with attached electric circuits. The concept of piezoelectric shunt damping can be attributed to Forward (1979), who was the first to reduce mechanical vibrations in optical systems by external inductive circuits.

Hagood and Flotow (1991) used resistive-inductive impedances for attenuating structural deformations. This may be interpreted as a very small tuned mass damper, as a system of second order, which interacts with the dynamics of a large system. In Schoeftner and Irschik (2009) and (2011b) conditions for the piezoelectric transducers and for the electric network are given such that the harmonic vibrations of an arbitrary force-excited laminated beam are completely annihilated.

The aforementioned citations have in common that a one-dimensional mathematical model of the piezoelectric beam is used to derive design specifications for shape control. Examples concerning the modeling of electromechanically coupled composite beams can be found in Zhou *et al.* (2005), Krommer and Irschik (2002) and Krommer (2001). In the latter contribution, the derived theory is compared to two-dimensional finite element plane stress calculations in ABAQUS. For passively controlled smart beams, a theory has been developed by Schoeftner and Irschik (2011a). Results for Timoshenko and Bernoulli-Euler beams are compared to two-dimensional plane-stress results in ANSYS. A discussion of simplified modeling of piezoelastic beams, e.g. the thermal analogy and the strain induced potential concepts, for free-vibrations can be found in Benjeddou (2009).

In this contribution we will deal with beams hosting span-wise constant piezoelectric transducers, which are also known as piezoelectric patches. An alternative method to reduce structural vibrations is the use of an array of electrically interconnected piezoelectric transducers on the substrate. Such a configuration when passive electrical impedances are in connection to adjacent transducers is treated in Vidoli and dell'Isola (2000), Porfiri and dell'Isola (2004) and dell'Isola *et al.* (2011). Its advantage is that patch actuators can be easily glued onto an elastic system and the resistor network can be removed or changed in order to optimize the damping performance. Such beam-patch models with interconnected resistive electric circuits may be interpreted as the discretization of a piezoelastic beam with so-called resistive electrodes, see

Schoeftner and Buchberger (2012) and Buchberger and Schoeftner (2013). In resistive electrodes the equipotential area condition over the electrodes is not fulfilled, i.e., the potential is not uniformly distributed and a voltage drop exists along the electrodes. It is found that a beam-type structure equipped with resistive electrodes of the piezo-transducers is governed by a system of two coupled partial differential equations. The first one extends the Bernoulli-Euler beam theory for a purely elastic beam by means of a voltage-dependent term, and the second one is a diffusion equation for the voltage distribution, with the time-derivative of the lateral deflection as the source term. The theory is verified by three-dimensional finite element calculations for highly, moderately and hardly conductive electrodes. Originally resistive electrodes and their combination with thin piezoelectric and pyroelectric films are used for touch- and lightpoint localization, see Buchberger *et al.* (2008a, 2009a, 2012a,b). To the best knowledge of the authors, coupled modeling of piezoelectric elements with resistive electrodes and elastic systems has been only performed by Rosi *et al.* (2010), where the sound radiation of a plate is reduced, and Lediaev (2010), where a finite element model of a bimorph cantilever based on a three-dimensional electromechanical formulation is presented.

A major drawback of commercial software packages like ANSYS and ABAQUS is that numerically efficient beam, plate and shell elements, which include the piezoelectric effect and the coupling to electrical impedances for active and passive applications, are currently not available. Even very simple mechanical configurations, like e.g., the cantilever beam with several patches treated in this contribution, may be set up as a three-dimensional object, thus three-dimensional solid elements have to be used, resulting in numerically inefficient simulation models. Thomas *et al.* (2009) present a finite element formulation of a mechanical structure equipped with several piezoelectric patches, where the electrical state of the piezoelectric patches is described by the voltage drop over the electrodes and the electric charge. Finally a reduced-order model of the problem is derived from the system's normal modes with all patches left short-circuited. A fully-coupled FE model for a laminated plate with embedded piezoelectric patches is developed in Godoy and Trindade (2011), which is used to optimize the locations of the patches and the design of the electric circuit. An extension to a vibroacoustic problem, where a piezoelectric plate with electric shunt circuits is coupled to the pressure field of a fluid is shown in Larbi, *et al.* (2012).

The paper is structured as follows: In the section 2 the basic equations of a smart slender beam are repeated, where we use the formulation of Krommer (2001) and Schoeftner and Irschik (2011a). In section 3 this theory is modified to obtain the differential equations for an elastic substrate hosting several piezoelectric patch actuators whose external electrodes are connected to the adjacent patches via resistors. In section 4 we present our shape control method based on our one-dimensional beam formulation. It is shown that a desired static deflection at several locations is obtained by the proper design of the resistors and the reference voltage source. The object under consideration is a tip-loaded cantilever. The validity of our method is only exact for static loads (section 5). As long as a certain non-dimensional parameter is small, which involves the number of the piezoelectric patches, the sum of the resistors in the electric network and the excitation frequency, the proposed shape control method is approximately fulfilled for dynamic excitations and for transient excitations of the force load (section 6 and 7). Furthermore, our one-dimensional results are compared to three-dimensional finite element results in ANSYS 12.0., demonstrating the validity of our proposed shape control method.

## 2. Lateral equation of motion of slender composite piezoelectric beams

In this section we summarize the governing equations of motion of a slender piezoelectric beam, which is composed of an elastic substrate ( $k = s$ ) and a lower and an upper piezoelectric layer ( $k = 1, u$ ). The beam is modeled as an equivalent single layer using classical laminate theory (CLT) within the framework of Bernoulli-Euler. For a detailed derivation of the governing equations and the physical assumptions, the reader is referred to Krommer (2001) and Schoeftner and Irschik (2011a). The coupled extensional and bending vibrations in the  $x$ - and the  $z$ -direction read\*

$$\begin{aligned} M_u(x)\ddot{u}_0(x) - M_{uw}(x)\ddot{w}_{0,x}(x) - N_{,x}(x) &= q_x(x), \\ \left[ M_{uw}(x)\ddot{u}_0(x) \right]_{,x} + M_w(x)\ddot{w}_0(x) - M_{,xx}(x) &= q_z(x). \end{aligned} \quad (1)$$

The axial and lateral displacements of the neutral fiber are denoted by  $u_0(x), w_0(x)$ , respectively, and the distributed loads along the beam axis and in the transverse direction by  $q_x(x), q_z(x)$ . The mass per unit length and the coupling inertia are denoted by

$$M_u(x) = M_w(x) = \sum_{k=s,u,l} \int_{z_{1k}}^{z_{2k}} \rho_k b_k(x) dz, \quad M_{uw}(x) = \sum_{k=s,u,l} \int_{z_{1k}}^{z_{2k}} \rho_k b_k(x) z dz, \quad (2)$$

where the variable width of each layer is  $b_k(x)$ . The thickness coordinates are  $z_{1k}, z_{2k}$ , the thickness of each layer is  $h_k = z_{2k} - z_{1k}$  and the mean distance to the  $x$ -axis is  $z_{mk} = (z_{2k} + z_{1k})/2$ . The vertical and lateral displacements of an arbitrary point of the beam is

$$u(x, z) = u_0(x) - zw_{0,x}(x), \quad w(x, z) = w_0(x). \quad (3)$$

The normal force and the bending moment can be divided into an elastic and an electrical portion

$$\begin{aligned} N(x) &= K_N(x)u_{0,x} - K_{NM}(x)w_{0,xx} + \sum_{k=u,l} \tilde{e}_{31}^k b_k(x) V^k \\ M(x) &= K_{NM}(x)u_{0,x} - K_M(x)w_{0,xx} + \sum_{k=u,l} \tilde{e}_{31}^k z_{mk} b_k(x) V^k. \end{aligned} \quad (4)$$

The axial stiffness  $K_N(x)$ , the coupling stiffness  $K_{NM}(x)$  and the bending stiffness  $K_M(x)$  are for a beam, which consists of a substrate and a lower and an upper piezoelectric layer

---

\*Although shape control of bending vibrations will be studied in this work, the coupled longitudinal-bending equations of a slender laminated beam are given here for the sake of completeness. It is noted that shape control of longitudinal vibrations is also possible. Similar equations to that presented in section 4 may be derived in a straightforward manner, but this is beyond the scope of this contribution and will be tackled in the future by the authors.

$$\begin{aligned}
 K_N(x) &= \sum_{k=s,u,l} \tilde{C}_{11}^k (z_{2k} - z_{1k}) b_k(x), \quad K_{NM}(x) = \sum_{k=s,u,l} \tilde{C}_{11}^k \frac{z_{2k}^2 - z_{1k}^2}{2} b_k(x) \\
 K_M(x) &= K_{M,elast}(x) + K_{M,piezo}(x) = \sum_{k=s,u,l} \tilde{C}_{11}^k \frac{z_{2k}^3 - z_{1k}^3}{3} b_k(x) + \sum_{k=u,l} \frac{(\tilde{e}_{31}^k)^2 (z_{2k} - z_{1k})^3}{12 \tilde{\kappa}_{33}^k} b_k(x).
 \end{aligned} \tag{5}$$

The variables  $\tilde{C}_{11}^k, \tilde{e}_{31}^k, \tilde{\kappa}_{33}^k$  denote the effective values of the Young's modulus, the piezoelectric transverse coefficient and the strain-free permittivity. The potential distribution inside the piezoceramic layer  $k$  depends on the external voltage supply  $V^k$

$$\varphi(x, z, t) = -\frac{V^k}{h_k} (z - z_{1k}) + \frac{\tilde{e}_{31}^k}{\tilde{\kappa}_{33}^k} w_{0,xx} \left( \frac{z^2}{2} - z_{mk} z \right) + \varphi(x, z_{1k}, t). \tag{6}$$

The electrical field is given by the relation  $E_z^k(x, z) = -\varphi_{,z}^k(x, z)$ . The electric displacement in the  $z$ -direction depends on the deformation and the applied voltage

$$D_z^k = \tilde{e}_{31}^k (u_{0,x} - z_{mk} w_{0,xx}) - \frac{\tilde{\kappa}_{33}^k}{h_k} V^k. \tag{7}$$

Integration over the electrode area of each layer  $A_k$  results into the total charge  $Q^k$

$$\begin{aligned}
 Q^k &= \int_0^l D_z^k b_k(x) dx = Q_{elast}^k - C^k V^k \\
 Q_{elast}^k &= \int_0^l \tilde{e}_{31}^k (u_{0,x} - z_{mk} w_{0,xx}) b_k(x) dx, \quad C^k = \frac{\tilde{\kappa}_{33}^k}{h_k} \int_0^l b_k(x) dx.
 \end{aligned} \tag{8}$$

The total length of the beam is denoted by  $l$ . Eq. (8) shows that one part of the total charge, namely the elastic part  $Q_{elast}^k$ , is generated by the deformation of the structure. The remaining part  $C^k V^k$  depends on the prescribed voltage over the electrodes and the capacitance of the piezoelectric layer  $C^k$ . It is noted that throughout this paper we do not account for piezoelectric or dielectric losses of the piezoelectric transducers. The components of the piezoelectric modulus and the permittivity matrix in Voigt notation (see Appendix B) are assumed to be frequency-independent and no static leakage current flow exists inside one piezoelectric element.

### 3. Lateral equations of motion for a beam with resistively interconnected piezoelectric patches

For the derivation of the equation of motions of an elastic beam, which is equipped with several piezoelectric patches, we can take advantage of Eqs. (1)-(8). These equations hold for a multi-layered piezoelectric beam with axially varying width. For reasons of simplification we assume a symmetrical setup around the  $x$ -axis, see Fig. 1, and that all piezoelectric patches have the same geometrical dimensions (length  $l_p$ , constant width  $b_p$  with  $k = p$  (piezo)). Thus it

follows that the coupling stiffness and the coupling mass are zero  $K_{NM} = M_{wv} = 0$ . Furthermore, we only allow external forces perpendicular to the beam axis  $q_x(x) = 0$ , therefore the axial deformation  $u_0(x)$  vanishes. Eq. (1) is reduced to

$$M_w \ddot{w}_0 + K_M w_{0,xxxx} = q_z(x). \quad (9)$$

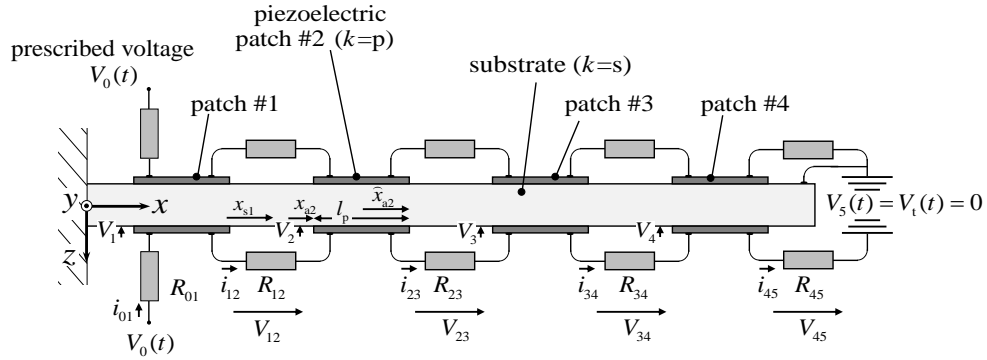


Fig. 1 Elastic cantilever hosting several piezoelectric patches. The voltage  $V_0(t)$  and the resistors  $R_{ij}$  are the same for upper and lower side and cause a voltage distribution of the piezoelectric patches. All inner electrodes and one link of the terminal resistance  $R_{45}$  are connected to ground

The bending stiffness is  $K_M = K_{M,elast} + K_{M,piezo}$  for  $x_{an} < x < x_{an} + l_p$ , where patch  $n$  is located, and  $K_M = K_{M,elast}$  otherwise. At  $x_{an}$  and  $\hat{x}_{an} = x_{an} + l_p$ , the continuity relations for the deflection, the rotation, the bending moment and the shear force read<sup>†</sup>

$$\begin{aligned} w_0(x_{an}^-) &= w_0(x_{an}^+) \\ w_{0,x}(x_{an}^-) &= w_{0,x}(x_{an}^+) \\ -K_{M,elast} w_{0,xx}(x_{an}^-) &= -(K_{M,elast} + K_{M,piezo}) w_{0,xx}(x_{an}^+) + 2\tilde{e}_{31} z_{mp} b_p V_n \\ -K_{M,elast} w_{0,xxx}(x_{an}^-) &= -(K_{M,elast} + K_{M,piezo}) w_{0,xxx}(x_{an}^+) \end{aligned} \quad (10)$$

and

$$\begin{aligned} w_0(\hat{x}_{an}^-) &= w_0(\hat{x}_{an}^+) \\ w_{0,x}(\hat{x}_{an}^-) &= w_{0,x}(\hat{x}_{an}^+) \\ -(K_{M,elast} + K_{M,piezo}) w_{0,xx}(\hat{x}_{an}^-) + 2\tilde{e}_{31} z_{mp} b_p V_n &= -K_{M,elast} w_{0,xx}(\hat{x}_{an}^+) \\ -(K_{M,elast} + K_{M,piezo}) w_{0,xxx}(\hat{x}_{an}^-) &= -K_{M,elast} w_{0,xxx}(\hat{x}_{an}^+). \end{aligned} \quad (11)$$

<sup>†</sup> The limits from below (left) and from above (right) at  $x_{an}$  are distinguished by  $x_{an}^-$  and  $x_{an}^+$ , respectively.

Eqs. (10) and (11) take into account that the voltage drops across the upper and lower patches are reversed in sign  $V_n = V_n^l = -V_n^u$ , therefore the factor 2 occurs in the voltage-dependent term in the third equations. Fig. 1 shows that the external electrodes of the piezoelectric patch  $n$  and  $n + 1$  are connected by the resistance  $R_{nn+1}$ . The current  $i_{nn+1}$ , which defines the current flow from patch  $n$  to patch  $n + 1$ , causes a voltage drop between the patch electrodes  $V_{nn+1} = V_n - V_{n+1}$ . From Kirchoff's voltage rule follows

$$V_n - R_{nn+1} i_{nn+1} = V_{n+1} \quad n = \{0, 1, \dots, N - 1, N\} \tag{12}$$

where  $N$  is the total number of patches. The currents from patch  $n$  to the adjacent patches  $n - 1$  and  $n + 1$ , denoted as  $i_{n-1n}$  and  $i_{nn+1}$ , have to be equal to the time derivative of the total charge generated by the piezoelectric patch  $n$ , see Eq. (8)

$$i_{nn+1} = i_{n-1n} = \dot{Q}_{nt} = \dot{Q}_{n,elast} = -C\dot{V}_n \quad n = \{1, 2, \dots, N\}$$

$$Q_{n,elast} = -\tilde{e}_{31} z_{mp} b_p [w_{0,x}(\tilde{x}_{an}) - w_{0,x}(x_{an})] \tag{13}$$

For the numerical example, we will use a beam with eight piezoelectric patch actuators  $N = 8$ . Combining Eqs. (12) and (13), we find nine algebraic equations and eight differential equations in order to determine the eight unknown voltage drops  $V_1, V_2, \dots, V_8$  and nine unknowns for the current flow  $i_{01}, i_{12}, \dots, i_{78}, i_{89}$ .

#### 4. Shape control of bending vibrations of a tip-loaded cantilever

In this section we give a criterion of how to choose the reference voltage  $V_0(t)$  and the resistors  $R_{ij}$  of the electric circuit, if a certain trajectory for the lateral displacement  $w_0(x_{sj})$  is required at location  $x_{sj}$ . The structure under investigation is a cantilever which is loaded by the tip-force  $F_0$ . We show that it is possible to calculate the necessary actuator voltages  $V_n(t)$  in the static case, in order to achieve a desired deformation at some selected locations. From a practical point of view, it is preferable to prescribe the voltage only at one piezoelectric patch, the voltage at the remaining patch actuators is achieved by the design of a proper electrical network to tune the voltage at each patch. For harmonic excitations or external loads with arbitrary time-dependence, we will show that the design rules computed for static shape control approximately hold in the dynamic regime, as long as a certain non-dimensional parameter is small. This parameter involves the resistors, the number of piezoelectric patches, their electric capacitances and the excitation frequency.

In the static case the governing equation in (9) can be integrated twice. The deformation due to the tip load and the voltage-induced deformation caused by the piezoelectric patches can be written as

$$w_0(x) = G_F(x)F_0 + \sum_{n=1}^N G_{Vn}(x)V_n, \tag{14}$$

where  $G_F(x)$  and  $G_{V_n}(x)$  are the solutions caused by the tip load acting at  $x = l$  and by the patch actuator  $n$  when the prescribed voltage is  $V_n = 1V$  over the electrodes. The patch  $n$  is located between the interval  $x_{an} \leq x < x_{an} + l_p$ . In order to simplify matters for a better understanding, we neglect the bending stiffness of the patch compared to those of the substrate  $K_{M, piezo} \ll K_{M, elast}$ .<sup>‡</sup> So the solutions  $G_F(x)$  and  $G_{V_n}(x)$  for a cantilever read

$$G_F(x) = \frac{1}{K_{M, elast}} \left( \frac{lx^2}{2} - \frac{x^3}{6} \right) \quad (15)$$

and

$$\begin{aligned} x < x_{an} : \quad & G_{V_n}(x) = 0 \\ x_{an} \leq x < x_{an} + l_p : \quad & G_{V_n}(x) = \frac{2\tilde{e}_{31}z_{mp}b_p}{K_{M, elast}} \frac{(x - x_{an})^2}{2} \\ x \geq x_{an} + l_p : \quad & G_{V_n}(x) = \frac{2\tilde{e}_{31}z_{mp}b_p}{K_{M, elast}} \left[ l_p (x - x_{an} - l_p) + \frac{l_p^2}{2} \right]. \end{aligned} \quad (16)$$

Since eight piezoelectric patches are used, the deformations at eight locations  $x_{si}$  can be prescribed.

These locations are situated between two adjacent patches and at the free end of the beam. Taking advantage of (15) and (16) one obtains the following linear equations

$$\begin{pmatrix} w_0(x_{s1}) \\ w_0(x_{s2}) \\ \vdots \\ w_0(x_{s8}) \end{pmatrix} = \begin{pmatrix} G_F(x_{s1}) & G_{V1}(x_{s1}) & G_{V2}(x_{s1}) & \cdots & G_{V8}(x_{s1}) \\ G_F(x_{s2}) & G_{V1}(x_{s2}) & G_{V2}(x_{s2}) & \cdots & G_{V8}(x_{s2}) \\ \vdots & \vdots & \vdots & \ddots & \vdots \\ G_F(x_{s8}) & G_{V1}(x_{s8}) & G_{V2}(x_{s8}) & \cdots & G_{V8}(x_{s8}) \end{pmatrix} \begin{pmatrix} F_0 \\ V_1 \\ V_2 \\ \vdots \\ V_8 \end{pmatrix}. \quad (17)$$

In matrix notation this reads

$$\underline{W}_0 = \underline{G}_F F_0 + \underline{G}_V \underline{V}. \quad (18)$$

One special goal of shape control is to completely annihilate the vibrations at certain locations, i.e.,  $\underline{W}_0 = \underline{0}$ . In this case the voltage vector is

<sup>‡</sup> It is noted that the patch stiffness is not neglected in the numerical example (sections 5, 6 and 7), although the thickness of the layers is only 5% of the substrate thickness, see Table 2. Eqs. (15) and (16) are only approximate solutions for the displacement under a unit force and under a unit voltage and have to be modified by accounting for the section-wise constant bending stiffness of the beam.

$$\underline{V} = -\underline{\underline{G}}_V^{-1} \underline{\underline{G}}_F F_0 \iff \underline{W}_0 = \underline{0}. \tag{19}$$

Substituting Eq. (16) into  $\underline{\underline{G}}_V$  results into a lower triangular matrix with nonzero diagonal elements for the cantilever, so the inverse matrix exists and a unique distribution for the voltage actuation of the piezoelectric patches is obtained. For static investigations the current through each electrical branch is equal, see Eqs. (12) and (13)

$$i = i_{01} = i_{12} = \dots = i_{78} = i_{89}, \tag{20}$$

since the piezoelectric capacitance  $C$  blocks the direct-current. In order to obtain the necessary patch voltage (19) one has to determine the resistance  $R_{01}, R_{12}, \dots, R_{78}, R_{89}$  such that

$$\frac{V_{n-1} - V_n}{V_n - V_{n+1}} = \frac{R_{n-1n}}{R_{nn+1}} \quad n = \{1, 2, \dots, 7, 8\} \tag{21}$$

holds. This means that in the static case the desired voltage is determined by the ratios of the resistors  $R_{n-1n} / R_{nn+1}$ . Since the left-hand side of Eq. (21) is known from Eq. (19), one has to fix the value of one arbitrary resistor in order to calculate the remaining ones.

### 5. Numerical results - static shape control of a tip-loaded cantilever

As a structural example, we simulate a cantilever beam subjected to the tip-force  $F_0$  in order to verify the above derived theoretical results. Table 2 in Appendix A lists the material parameters and the geometry of the beam configuration, see Fig. 2. The cantilever hosts eight actuator patches with length  $l_p$ , the width of the substrate and of the patches are equal  $b_s = b_p = 0.05$  m. The one-dimensional calculation is based on Eqs. (9), (12) and (13). We discretize the beam equation (9) by using

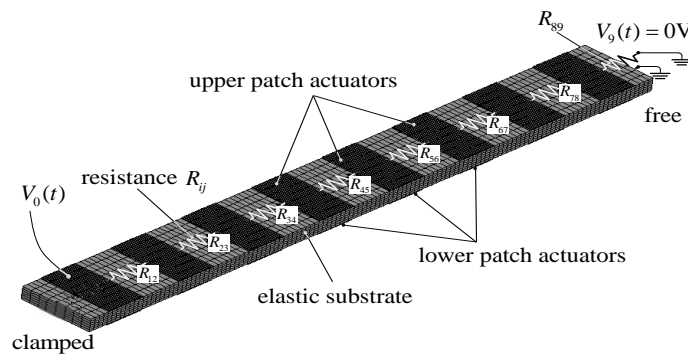


Fig. 2 Three-dimensional finite element model of a cantilever with distributed patch actuators (ANSYS). The voltage at each patch depends on the nominal voltage  $V_0(t)$ , on the terminal voltage  $V_9(t) = 0$  and on the resistors  $R_{ij}$

Bernoulli-Euler beam elements and by accounting for the kinematic and dynamic boundary conditions of each finite element given in Eqs. (10) and (11).

The beam is divided into 34 finite elements. The self-written one-dimensional code for the beam elements is written in MATLAB, which takes into account the coupling of the discretized model of the piezoelectric beam and the electrical Eqs. (12) and (13), in order to obtain a state-space representation. For the transient simulation results, which are shown in section 7, the system matrices are imported into the Simulink environment. The three-dimensional finite element simulation is performed in ANSYS 12.0. The substrate is divided into 96 elements in the axial direction, 6 elements in the thickness direction and 8 elements in the lateral direction. The patches consist of 16, 4 and 8 elements in the axial, thickness and lateral direction. The coupled-field solid element SOLID5 is used which provides three structural degrees of freedom for the deformation and optionally one electrical degree of freedom (electric potential) for modeling the piezoelectric patches.

The electrical resistances  $R_{12}, R_{23}, \dots, R_{78}, R_{89}$ , are modeled by CIRCU94 elements. They connect the voltage degrees of freedom at the external electrodes at  $z = \pm 4.4$  mm. The inner electrodes of the patches at  $z = \pm 4.4$  mm and the terminal load  $V_9$  are grounded. The material parameters for the piezoelectric transducers (PZT-5A) and the substrate (Aluminum) are given in Appendix A. The equivalent one-dimensional material constants for the one-dimensional beam model are obtained by applying the transformation rules presented in Schoeftner and Irschik (2011a). Furthermore, the modal damping coefficient  $d = 0.02$  is assumed in both the ANSYS and the Bernoulli-Euler model.

Our first aim is to completely suppress the static deflection at the positions  $x_{si}$  (Table 2), which are situated between two adjoining patches and at the free end. In a first step, Eq. (19) is solved to calculate the required patch voltages. The maximum voltage is used as the reference voltage signal, thus  $V_0 = V_l = 250.3$  V holds. Using Eq. (21) and fixing the total resistance of all resistors  $R_{total} = 1000\Omega$ , one finds the values of the resistors, see Table 1. The static deflection and the voltage distributions are shown in Fig. 3 for the one-dimensional (Bernoulli-Euler) and in Fig. 4 for the three-dimensional model (ANSYS). The deflection as a function of the beam length is plotted in Figs. 3(a) and 3(b). The tip deflection of the beam subjected to the tip-load (light gray-  $F_0 = 1$  N,  $V_0 = 0$  V:  $w_0(l) = 0.2415$  mm) is the same, but with opposite sign as the deflection of the beam under the optimal electrical load (black-  $F_0 = 0$  N,  $V_0 = 250.3$  V:  $w_0(l) = -0.2415$  mm). If the external and the electrical load act simultaneously, the deflection is completely annihilated at the 8 desired sensor locations  $x_{si}$ .

For the ANSYS model the same values in the electrical network and the same reference voltage are used. It is clear that the design Eqs. (19) and (21) for shape control will only be approximately fulfilled in the three-dimensional case. The outcome of our calculations in ANSYS is plotted in Fig. 4. The shear stress  $\tau_{xz} = F_0 / (b_s h_s)$  acts as the external load at the free end, which is equivalent to the tip-force  $F_0$  in the one-dimensional model. The deflections deviate slightly from the Bernoulli-Euler results:  $w_0(l) = 0.2386$  mm (light gray) and  $w_0(l) = -0.2329$  mm (black). Superposing mechanical and electrical loads, one finds that the tip-deflection is strongly attenuated  $w_0(l) = 0.0057$  mm. The remaining residual displacement with our shape-control method is rather small compared to the tip-force deflection (approximately 2%).

Table 1 Values for the resistors (total resistance  $R_{tot} = \sum R_{ij} = 1000\Omega$ )

resistor (unit)	value	resistor (unit)	value	resistor (unit)	value
$R_{01} (\Omega)$	0	$R_{12} (\Omega)$	177.57	$R_{23} (\Omega)$	83.70
$R_{34} (\Omega)$	176.81	$R_{45} (\Omega)$	82.72	$R_{56} (\Omega)$	177.36
$R_{67} (\Omega)$	82.99	$R_{78} (\Omega)$	177.36	$R_{89} (\Omega)$	41.49

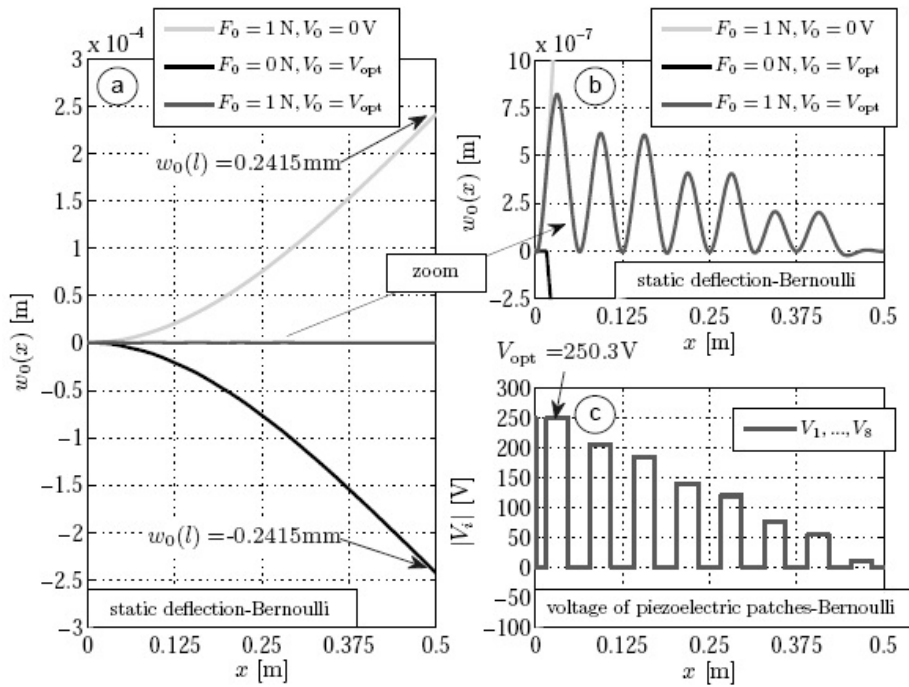


Fig. 3 (a), (b) Results of the static deflection with Bernoulli-Euler finite elements when the beam is subjected to the tip-force  $F_0$  only (light gray), to the optimal voltage distribution only (black) or to the tip-force and the optimal voltage distribution for shape control and (c) Voltage distribution  $V_1, \dots, V_8$  across the electrodes of each patch generated by  $V_0$  and the electric circuit resistors  $R_{ij}$

Next we show a robustness and sensitivity analysis, which is important from an engineering point of view to find sensitive variables that may affect the performance of the system. Especially the influence of the resistors is important because of the finite precision of the ohmmeter to tune the potentiometer. Fig. 5 shows the shape control results, if either the resistors values are rounded to the nearest integer ( $R_{ij} = [0, 178, 84, 177, \dots, 177, 41]\Omega$ , light gray), if either the reference voltage is raised by 1% ( $V_0 = 252.8\text{V}$ , gray dashdot), or if the patch positions are shifted to the left (1 mm,

black). The deviation from the optimal curve (gray) is rather small for all three cases. Even if the voltage is overestimated by 1%, the tip-deflection is approximately 1/100 compared to the non-controlled beam deflection:  $w_0(l) = -0.0024$  mm.

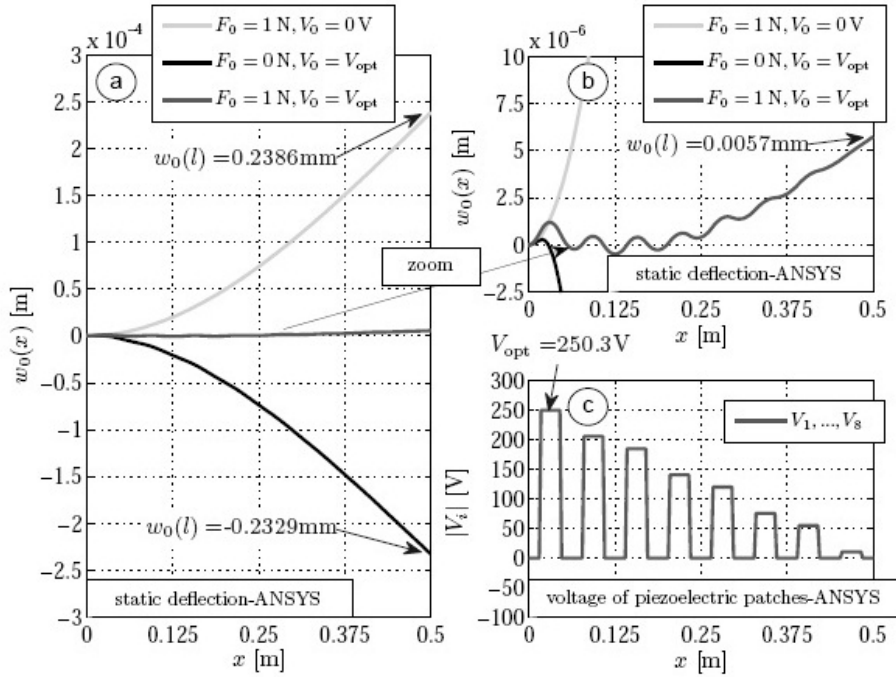


Fig. 4 (a), (b) Results of the static deflection with the ANSYS model when the beam is subjected to the tip-force  $F_0$  only (light gray), to the optimal voltage distribution only (black) or to the tip-force and the optimal voltage distribution for shape control and (c) Voltage distribution  $V_1, \dots, V_s$  across the electrodes of each patch generated by  $V_0$  and the electric circuit resistors  $R_{ij}$

## 6. Numerical results - dynamic shape control of a tip-loaded cantilever

The deflection of a beam will be also approximately annihilated at the sensor positions, if the beam is loaded by the harmonic force  $F(x, t) = F_0 \sin \omega t$ . Again, the one- and three-dimensional models are used and the frequency response  $\hat{w}_0(x, \omega)$  is calculated for a beam subjected to the tip-force only, to the electrical voltage only and to both of them, the superposition of mechanical and electrical loads. The same electrical circuit is used as in the static case (see Table 1 for the resistors  $R_{ij}$ ). Since only the ratios of the resistors, but not total resistance  $R_{tot}$ , are important in the static case, see Eq. (21), the influence of the absolute values of the resistors for transient excitations is discussed in section 7. Results are shown in Fig. 6 (Bernoulli-Euler FE) and in Fig. 7 (ANSYS). The tip-deflection and the displacement at  $x = 0.125$  m as a function of the excitation frequency are depicted in Figs. 6(a) and 6(b). If the shape control technique is applied (gray curve),

the deflection at the free end approaches zero  $\hat{w}_0(l, \omega \rightarrow 0) \rightarrow 0$  m for excitations of low-frequency. For higher frequencies the deflection is reduced by two orders of magnitude for frequencies below  $f < 50$  Hz. The tip-deflection at the first natural frequency  $f_1 = 26.5$  Hz are  $\hat{w}_0(l, \omega_1) = 5.9 \times 10^{-3}$  m (tip-force) and  $\hat{w}_0(l, \omega_1) = 3.1 \times 10^{-5}$  m (shape control), respectively. The system responses of the force- and voltage-loaded beams are not exactly equal in the dynamic case due to the leakage current across the piezoelectric (see the discussion in section 7, in Figs. 7 and 8).

Nevertheless, close to the second eigenfrequency at  $f_2 = 166.5$  Hz the deflection is reduced approximately to 22% of the force-loaded beam:  $\hat{w}_0(l, \omega_2) = 15.8 \times 10^{-5}$  m (tip-loaded) and  $\hat{w}_0(l, \omega_2) = 3.5 \times 10^{-5}$  m (shape control). In the range of the first and the second eigenfrequency, the deformation is calculated as a function of the axial coordinate, see Figs. 6(c) and 6(d). As already mentioned before, the peaks are attenuated well for the first mode, but also the second mode is well damped.

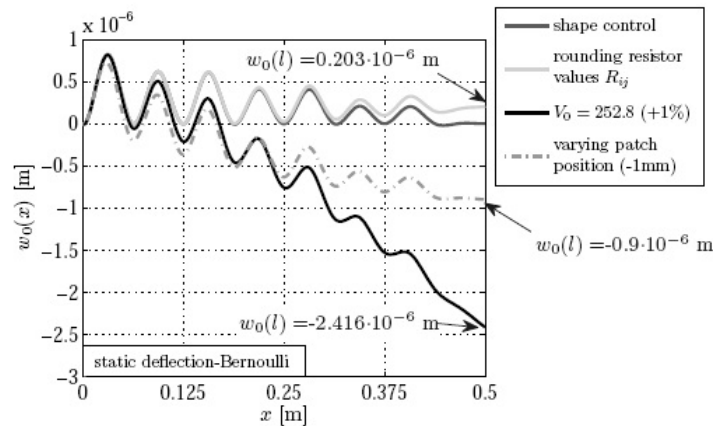


Fig. 5 (a), (b) Sensitivity analysis of the static shape control results with Bernoulli-Euler finite elements: rounding of the resistor values  $R_{ij}$  to next integer (light gray), increasing the reference voltage by 1% to  $V_0 = 252.8$ V (black) and changing the position of the piezoelectric patches (gray-dashdot)

The ANSYS results in the dynamic frequency range, see Fig. 7, are qualitatively similar to the Bernoulli-Euler FE beam results. Close to the first eigenfrequency at  $f_1 \approx 26.7$ Hz the tip-deflection response of the controlled beam is 1.9% of the mechanically loaded beam:  $\hat{w}_0(l, \omega_1) = 5.8 \times 10^{-3}$  m (tip-loaded) and  $\hat{w}_0(l, \omega_1) = 1.1 \times 10^{-4}$  m (shape control). At higher frequencies, the technique for shape control is less efficient. The peak at the second eigenfrequency is  $\hat{w}_0(l, \omega_2) = 3.7 \times 10^{-5}$  m, which is a reduction of two-thirds of the tip-loaded

deflection of  $\hat{w}_0(l, \omega_2) = 11 \times 10^{-5}$  m. The attenuation is still in the range which has been obtained with the simpler one-dimensional theory.

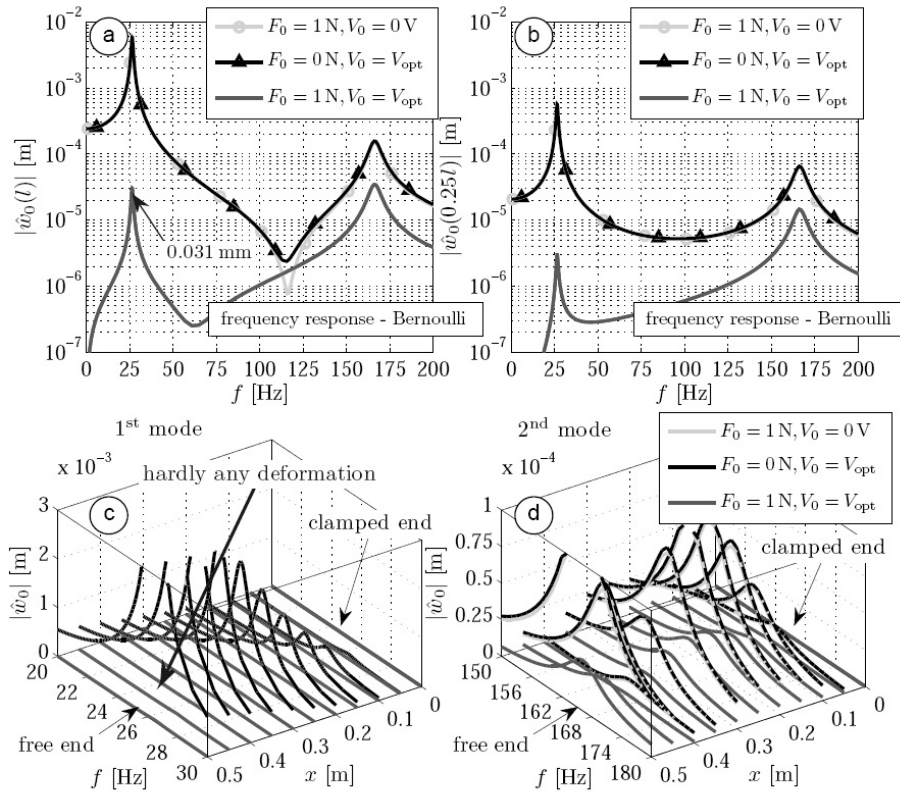


Fig. 6 (a), (b) Frequency response  $\hat{w}_0(l)$  and  $\hat{w}_0(0.25l)$  with Bernoulli-Euler finite elements due to the tip-force excitation (light gray), due to voltage actuation (black) and under shape control (gray), (c) Deflection of the beam close to the first resonance at  $f_1 \approx 26.5$  Hz and (d) Deflection of the beam close to the second resonance at  $f_1 \approx 166.5$  Hz

## 7. Limitations of dynamic shape control with resistive circuits and discussion of the energy consumption

Fig. 6 (Bernoulli-Euler FE) shows that for low-frequency excitations, the displacement is not totally annihilated by our proposed shape control method. Especially for higher excitation frequencies, the damping performance is less than for low-frequency excitations. The physical explanation for this discrepancy is the leakage current through the piezoelectric patches that is modeled as a capacitance, which has to be kept as small as possible. This is achieved by either using piezoelectric transducers with low permittivity  $\tilde{\kappa}_{33}^p$ , and thus a low piezoelectric

capacitance  $C_p$ , or by choosing low-resistances for the network. The first possibility is preferred since the consumed electrical energy is inversely proportional to the resistance. In the static case, the electrical power needed to compensate a tip-force of 1N is  $P_{elec} = V_0^2 / R_{tot} \approx 62.7 \text{ W}$ , with  $V_0 = 250.3\text{V}$  and  $R_{tot} = 1\text{k}\Omega$ , see Eq. (19). So for practical reasons, one has to keep in mind that the reference voltage and the current through the electrical loads  $R_{ij}$  must not fall below a critical value, otherwise the electrical components may be destroyed. In general, the maximal current of the voltage amplifier for the piezoelectric patches is limited to some 100 mA, meaning that the total resistance of network is limited downwards. In the following we derive a criterion for the validity of our shape control method for higher frequencies.

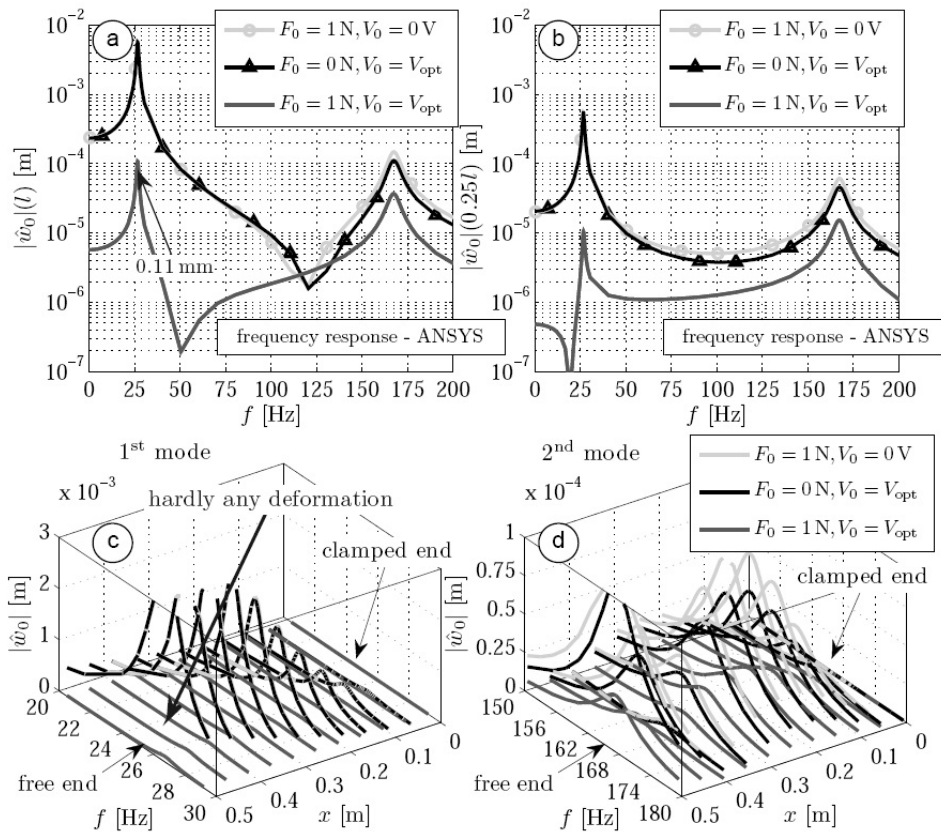


Fig. 7 (a), (b) Frequency response  $\hat{w}_0(l)$  and  $\hat{w}_0(0.25l)$  with the ANSYS model due to the tip-force excitation (light gray), due to the voltage actuation (black) and under shape control (gray), (c) Deflection of beam close to the first resonance at  $f_1 \approx 26.7 \text{ Hz}$  and (d) Deflection of beam close to the second resonance at  $f_2 \approx 167.5 \text{ Hz}$

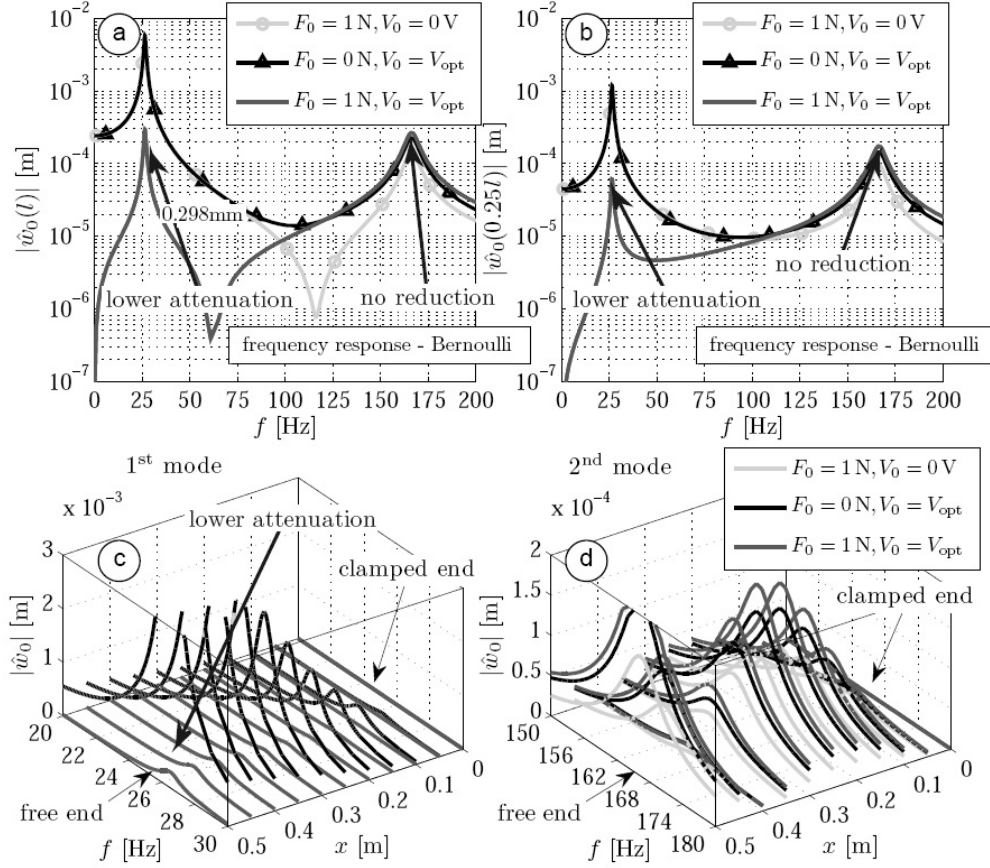


Fig. 8 (a), (b) Frequency response  $\hat{w}_0(l)$  and  $\hat{w}_0(0.25l)$  with Bernoulli-Euler finite elements due to the tip-force excitation (light gray), due to voltage actuation (black) and under shape control, but with a higher non-dimensional parameter  $\pi_1 = 1.072$  for  $f = 26.5$  Hz (gray), (c) Deflection of the beam close to the first resonance  $f \approx 26.5$  Hz and (d) Deflection of beam close to the second resonance at  $f \approx 166$  Hz

If we demand low lateral deformations  $w_0(x)$ , the order of the slope is also low  $O(w_{0,x}(x)) \approx 0$ , and therefore the elastic current  $Q_{n,\text{elast}}$  is negligible in (13). Combining (12) and (13), one obtains

$$\frac{V_0 - V_1}{\alpha_{01}} - \frac{V_4 - V_t}{\alpha_{4t}} = CR_{\text{tot}} (\dot{V}_1 + \dots + \dot{V}_8). \quad (22)$$

In (22)  $\alpha_{01}$  and  $\alpha_{4t}$  are defined as the ratios  $\alpha_{01} = R_{01}/R_{\text{tot}}$  and  $\alpha_{4t} = R_{4t}/R_{\text{tot}}$ , where the denominator is the sum of all resistors. The right-hand side is the leakage current through all piezoelectric capacitances.

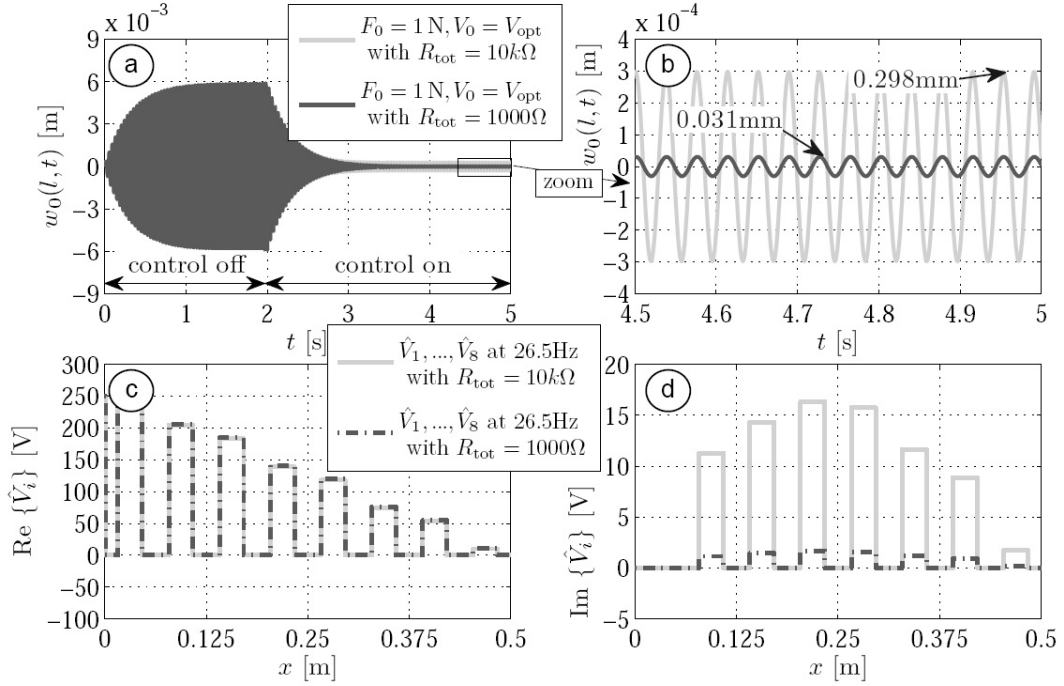


Fig. 9 (a), (b) Transient frequency response with and without control due to the tip-force  $F_0(t) = \sin(26.5 \cdot 2\pi t)$  for the highly resistive circuit ( $R_{tot} = 1000\Omega$  or  $\pi_1 = 0.107$ , gray-high attenuation) and for the low-ohmic circuit ( $R_{tot} = 10k\Omega$  or  $\pi_1 = 0.072$ , light gray-lower attenuation), (c) and (d) Real and imaginary parts of the voltage distribution  $V_i$  of each patch

If Eq. (22) is divided by the reference voltage  $V_0$ , we find that the non-dimensional number  $\pi_1$  should be smaller than one. For our numerical example this reads

$$\pi_1 := O\left(CR_{total} \frac{\dot{V}_1 + \dots + \dot{V}_s}{V_0}\right) = 8CR_{tot}\omega = \tau\omega \ll 1 \quad (23)$$

If this criterion is fulfilled, i.e., the time constant  $\tau$  of the electric system is small, our shape control technique is successful for a certain excitation frequency  $\omega$ . Eq. (23) depends on the piezoelectric capacitance, on the sum of the resistances, on the number of patch actuators and on the excitation frequency. This means that for high excitation frequencies, the resistor values of the electric circuit should be small.

Results for the total resistance of  $R_{tot} = 10k\Omega$  (i.e.,  $\pi_1 = 1.072$  at  $f = 26.5$  Hz), which is ten times higher than in the previous case, are drawn in Figs. 8 and 9. If the excitation frequency exceeds  $f = 75$  Hz, hardly any attenuation of the deflection takes place, see Figs. 8(a) and 8(b).

At the first eigenfrequency, the tip deflection is reduced  $\hat{w}_0(L, \omega_1) = 0.298 \times 10^{-3}$  m, whereas the deflection is even amplified at the second eigenfrequency. This is a very important outcome of our study: in the dynamic case, especially for high-frequency excitations, one has to take care that, beside the validity of Eq. (21) for the resistor ratios, the absolute values of the resistors are not too high. So the non-dimensional relation  $\pi_1 < 1$  can be considered as an upper limit for the design of the resistive network. For  $\pi_1 > 5$  the proposed shape control method simply fails and the results may be even worse than without applying this method.

For the transient simulation, the tip-load  $F(x, t) = \sin(26.5 \cdot 2\pi t)$  acts on the beam (Figs. 9(a) and 9(b)). We compare the results with  $R_{tot} = 1000 \Omega$  (low resistances-  $\pi_1 = 0.107$ ) and  $R_{tot} = 10 \text{ k}\Omega$  (high resistances-  $\pi_1 = 1.072$ ). After two seconds, the control is switched on, see Fig. 9. In the steady-state the maximum remaining deformation are  $0.031 \times 10^{-3}$  m and  $0.298 \times 10^{-3}$  m, respectively. Comparing the real and the imaginary parts of the voltage at this frequency (Figs. 9(c) and (d)), one sees that the imaginary part is higher for the highly resistive circuit. The maximum value at the fourth patch of 16.6V is significantly higher than for the low resistive circuit 1.7 V.

## 8. Conclusions

In this paper we present a theory for an elastic slender beam hosting several piezoelectric transducers which are connected by resistors. To this end we extend the Bernoulli-Euler beam theory, which leads to a partial differential equation coupled to a set of ordinary differential equations for the electrical part. Based on the derived equations, we find that the lateral deformation of a tip-loaded cantilever at specified locations along the beam axis can be prescribed, if the resistors are properly tuned and if a certain reference voltage signal is applied across the electrodes of one piezoelectric patch. The derived shape control method is validated by a clamped-free beam with eight piezoelectric patches, which is subjected to a tip-load. Two simulation models are set up: First the derived beam equations are discretized with Bernoulli-Euler elements in order to obtain a one-dimensional model. The second model is a three-dimensional finite element model in ANSYS 12.0. It is shown that in the static case, the deflections of the model based on the Bernoulli-Euler theory are exactly annihilated at the desired locations, whereas in the ANSYS model the lateral deflections are approximately nullified under our shape control conditions. A frequency response analysis and a transient simulation show that our control method is suitable for the high frequency range, as long as a certain non-dimensional parameter, involving the capacitance and the number of the piezoelectric patches, the total resistance and the excitation frequency of the external load, is small. A major challenge in the future will be to generalize the presented theory of shape control to take into account arbitrary boundary and external loading conditions, transient force loads, force couples and distributed loads and non-zero values of the displacement for trajectory control, in order to develop algorithms and design criteria for impedances of the network.

## Acknowledgements

The research was funded by the COMET K2-Center ACCM and the Austrian Research Promotion Agency (FFG) under the contract number 825348/K-Licht.

## References

- Agrawal, B.N. and Treanor, K.E. (1999), "Shape control of a beam using piezoelectric actuators", *Smart Mater. Struct.*, **8**, 729-740.
- Benjeddou, A. (2009), "New insights in piezoelectric free-vibrations using simplified modeling and analyses", *Smart Struct. Syst.*, **5**(6), 591-612.
- Buchberger, G., Schwoediauer, R. and Bauer, S. (2008a), "Flexible large area ferroelectret sensors for location sensitive touchpads", *Appl. Phys. Lett.*, **92**, 123511 (3 pp).
- Buchberger, G., Schwoediauer, R., Arnold, N. and Bauer, S. (2008b), "Cellular ferroelectrets for flexible touchpads, keyboards and tactile sensors", *Proceedings of the IEEE Sensors Conference 2008*.
- Buchberger, G., Bartu, P., Schwoediauer, R., Jakoby, B., Hilber, W. and Bauer, S. (2012a), "A flexible polymer sensor for light point localization", *Procedia Eng.*, **47**, 795-800.
- Buchberger, G., Schoeftner, J., Schwoediauer, R., Jakoby, B., Hilber, W. and Bauer, S. (2012b), "Modeling of large-area sensors with resistive electrodes for passive stimulus-localization", accepted for publication *Sensor Actuat. A-Phys.*
- Buchberger, G. and Schoeftner, J. (2013), "Modeling of slender laminated piezoelastic beams with resistive electrodes - comparison of analytical results with three-dimensional finite element calculations", *Smart Mater. Struct.*, **22**(3), 032001 (13pp).
- dell'Isola, F., Maurini, C. and Porfiri, M. (2011), "Passive damping of beam vibrations through distributed electric networks and piezoelectric transducers: prototype design and experimental validation", *Smart Mater. Struct.*, **13**(2), 299-308.
- Forward, R. L. (1979), "Electronic damping of vibrations in optical structures", *Appl. Optics.*, **18**(5), 690-697.
- Godoy, T.C. and Trindade, M.A. (2011), "Modeling and analysis of laminate composite plates with embedded active-passive piezoelectric networks", *J. Sound Vib.*, **330**(2), 194-216.
- Hafka, R.T. and Adelman, H.M. (1985), "An analytical investigation of shape control of large space structures by applied temperatures", *AIAA J.*, **23**(3), 450-457.
- Hagood, N.W. and Flotow, A. (1991), "Damping of structural vibrations with piezoelectric materials and passive electrical networks", *J. Sound Vib.*, **146**(2), 243-268.
- Hubbard, J.E. and Burke, S.E. (1992), *Distributed transducer design for intelligent structural components*, in: *Intelligent Structural System*, (Eds. H.S. Tzou and G.L. Anderson), Kluwer Academic Publishers, Norwell.
- Irschik, H., Krommer, M., Belyaev, A.K. and Schlacher, K. (1998), "Shaping of piezoelectric sensors/actuators for vibrations of slender beams: coupled theory and inappropriate shape functions", *J. Intel. Mat. Syst. Struct.*, **9**(7), 546-554.
- Irschik, H. (2002), "A review on static and dynamic shape control of structures by piezoelectric actuation", *Eng. Struct.*, **24**(1), 5-11.
- Irschik, H., Krommer, M. and Pichler, U. (2003), "Dynamic shape control of beam-type structures by piezoelectric actuation and sensing", *Int. J. Appl. Electrom.*, **17**(1-3), 251-258.
- Krommer, M. (2001), "On the correction of the Bernoulli-Euler beam theory for smart piezoelectric beams", *Smart Mater. Struct.*, **10**(4), 668-680.
- Krommer, M. and Irschik, H. (2002), "An electromechanically coupled theory for piezoelastic beams taking into account the charge equation of electrostatics", *Acta Mech.*, **154**(1-4), 141-158.
- Larbi, W., Deü, J.F. and Ohayon, R. (2012), "Finite element formulation of smart piezoelectric composite plates coupled with acoustic fluid", *Compos. Struct.*, **94**(2), 501-509.
- Lediaev, L. (2010), *Finite element modeling of piezoelectric bimorphs with conductive polymer electrodes (Doctoral thesis Montana State University)*, Bozeman, Montana.

- Nader, M. (2007), *Compensation of vibrations in smart structures: shape control, experimental realization and feedback control (doctoral thesis Johannes Kepler Universitaet Austria)*, Trauner Verlag, Linz.
- Porfiri, M. and dell'Isola, F. (2004), "Multimodal beam vibration damping exploiting PZT transducers and passive distributed circuits", *J. Phys. IV*, **115**, 323-330.
- Rosi, G., Pouget, J. and dell'Isola, F. (2010), "Control of sound radiation and transmission by a piezoelectric plate with an optimized resistive electrode", *Eur. J. Mech. A - Solid*, **29**(5), 859-70.
- Schoeftner, J. and Irschik, H. (2009), "Passive damping and exact annihilation of vibrations of beams using shaped piezoelectric layers and tuned inductive networks", *Smart Mater. Struct.*, **18**(12), 125008 (9pp).
- Schoeftner, J. and Irschik, H. (2011a), "A comparative study of smart passive piezoelectric structures interacting with electric networks: Timoshenko beam theory versus finite element plane stress calculations", *Smart Mater. Struct.*, **20**(2), 025007 (13 pp).
- Schoeftner, J. and Irschik, H. (2011b), "Passive shape control of force-induced harmonic lateral vibrations for laminated piezoelectric Bernoulli-Euler beams-theory and practical relevance", *Smart Struct. Syst.*, **7**(5), 417-432.
- Schoeftner, J. and Buchberger, G. (2012), "An electromechanically-coupled Bernoulli-Euler beam theory taking into account the finite conductivity of the electrodes for sensing and actuation", *Proceedings of the 2012 World Congress on Advances in Civil, Environmental, and Material Research (ACEM'12): CD-ROM*, (Ed. Chang-Koon Choi), 1051-65, 8-2012, Seoul, South Korea.
- Thomas, O., Deü, J.F. and Ducarne, J. (2009), "Vibrations of an elastic structure with shunted piezoelectric patches: efficient finite element formulation and electromechanical coupling coefficients", *Int. J. Numer. Meth. Eng.*, **80**(2), 235-268.
- Vidoli, S. and dell'Isola, F. (2000), "Modal coupling in one-dimensional electro-mechanical structured continua", *Acta Mech.*, **141**(1-2), 37-50.
- Zhou, Y.G., Chen, Y.M. and Ding, H.J. (2005), "Analytical solutions to piezoelectric bimorphs based on improved FSDT beam model", *Smart Struct. Syst.*, **1**(3), 309-324.

## Appendix A

For the numerical case study the material parameters and the geometrical dimensions (Aluminum for the substrate with index s, PZT-5A for the piezoelectric patch with index p) are listed in Table 2. The effective piezomodulus, the modulus of elasticity and the strain-free permittivity are obtained from the values given in Appendix B by taking advantage of the transformation rules, see Schoeftner and Irschik (2011a).

## Appendix B

Material properties of PZT-5A:

- Density:  $\rho_p = 7750 \text{ kgm}^{-3}$
- Elasticity components in Voigt notation  $C_{11} = C_{22} = 123 \times 10^9 \text{ Nm}^{-2}$ ,  $C_{12} = 76.7 \times 10^9 \text{ Nm}^{-2}$ ,  $C_{13} = C_{23} = 70.3 \times 10^9 \text{ Nm}^{-2}$ ,  $C_{33} = 97.1 \times 10^9 \text{ Nm}^{-2}$ ,  $C_{44} = C_{55} = 22.3 \times 10^9 \text{ Nm}^{-2}$ ,  $C_{66} = 0.5(C_{11} - C_{12}) = 23.15 \times 10^9 \text{ Nm}^{-2}$ , else  $C_{ij} = 0 \text{ Nm}^{-2}$
- Components of piezoelectric modulus in Voigt notation:  $e_{31} = e_{32} = -7.15 \text{ Asm}^{-2}$ ,  $e_{33} = 13.7 \text{ Asm}^{-2}$ ,  $e_{24} = e_{15} = 11.9 \text{ Asm}^{-2}$ , else  $e_{ij} = 0 \text{ Asm}^{-2}$
- Components of permittivity in Voigt notation:  $\kappa_{11} = \kappa_{22} = 1649 \times \varepsilon_0$ ,  $\kappa_{33} = 1750 \times \varepsilon_0$  with  $\varepsilon_0 = 8.854 \times 10^{-12} \text{ AsV}^{-1} \text{ m}^{-1}$ , else  $\kappa_{ij} = 0 \text{ AsV}^{-1} \text{ m}^{-1}$

Table 2 Parameters used in the numerical example

variable (unit)	value	variable (unit)	value
$\rho_p (\text{kgm}^{-3})$	7750	$\rho_s (\text{kgm}^{-3})$	2700
$z_{1p} (\text{m})$	$4.00 \times 10^{-3}$	$z_{2p} (\text{m})$	$4.40 \times 10^{-3}$
$z_{1s} (\text{m})$	$-4.00 \times 10^{-3}$	$z_{2s} (\text{m})$	$4.00 \times 10^{-3}$
$l (\text{m})$	0.5	$l_p (\text{m})$	0.03
$\tilde{\kappa}_{33}^p (\text{AsV}^{-1} \text{ m}^{-1})$	$2.15 \times 10^{-8}$	$\tilde{e}_{31}^p (\text{Asm}^{-2})$	-10.94
$\tilde{C}_{11}^p (\text{Nm}^{-2})$	$6.29 \times 10^{10}$	$\tilde{C}_{11}^s (\text{Nm}^{-2})$	$7.22 \times 10^{10}$
$x_{ai} (\text{m})$	$0.01625 + l \times (i-1)/8$	$x_{si} (\text{m})$	$l \times i/8$
$b_s (\text{m})$	0.05	$b_p (\text{m})$	0.05
$C (\text{AsV}^{-1})$	$8.05 \times 10^{-8}$	$F_0 (\text{N})$	1